

# Adaptive Assignment for Geometry Aware Local Feature Matching

Dihe Huang, Ying Chen, Shang Xu, Yong Liu, Wenlong Wu, Yikang Ding,  
Chengjie Wang, Fan Tang

**Abstract.** Local image feature matching, aiming to identify and correspond similar regions from image pairs, is an essential concept in computer vision. Most existing image matching approaches follow a one-to-one assignment principle and employ mutual nearest neighbor to guarantee unique correspondence between local features across images. However, images from different conditions may hold large-scale variations or viewpoint diversification so that one-to-one assignment may cause ambiguous or missing representations in dense matching. In this paper, we introduce AdaMatcher, a novel detector-free local feature matching method, which first correlates dense features by a lightweight feature interaction module and estimates co-visible area of the paired images, then performs a patch-level many-to-one assignment to predict match proposals, and finally refines them based on a one-to-one refinement module. Extensive experiments show that AdaMatcher outperforms solid baselines and achieves state-of-the-art results on many downstream tasks. Additionally, the many-to-one assignment and one-to-one refinement module can be used as a refinement network for other matching methods, such as SuperGlue, to boost their performance further. Code will be available upon publication.

**Keywords:** image matching, sub-pixel refinement, many-to-one assignment

## 1 Introduction

Establishing accurate correspondences for local features between image pairs is an essential basis for a broad range of computer vision tasks, including visual localization, structure from motion (SfM), simultaneous localization and mapping (SLAM), etc. However, achieving reliable and accurate feature matching is still challenging due to various factors such as scale changes, viewpoint diversification, illumination variations, repetitive patterns, and poor texture.

Conventional feature matching pipelines relied on geometry and appearance invariant local features to establish putative matches, followed by one-to-one matching criterion (*e.g.*, mutual ratio test [22]) and geometric verification (*e.g.*, RANSAC) to filter outliers. On the one hand, appearance invariance usually resorts to CNN-based architectures that incorporate rich semantic information. On the other hand, local geometry deformation is parameterized by scale/viewpoint adaptation, while more recently, by a data-driven approach [9]. However, no solid

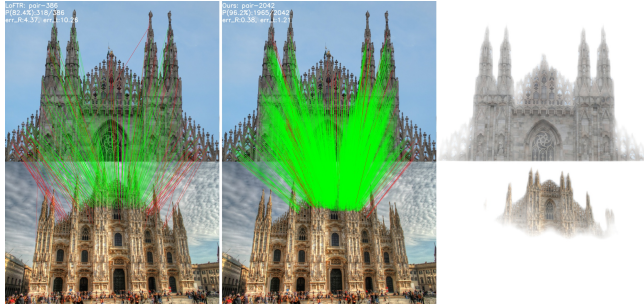


Fig. 1: **Comparison between the proposed method AdaMatcher and LoFTR.** This example demonstrates that AdaMatcher is capable of generating more robust and accurate matches using adaptive assignment and co-visible area segmentation, compared with SOTA matching method LoFTR [33].

solution has been available for this notorious geometry invariance issue until now. Hand-crafted local features such as SIFT [22] or ORB [28] adopt scale-space theory [20] to alleviate potential large scale variations. However, overwhelming noise will be introduced when scale or viewpoint varies tremendously, hampering the robustness of geometry-invariance feature representations. CNNs inherently possess inductive bias of translation equivariance and locality, which are suitable for extracting local features. However, neither scale-viewpoint alignment [6, 35] as the preprocessing module nor multi-scale feature extraction [14, 23, 25] may introduce complicated design and excessive computation. Nevertheless, scale and viewpoint invariant feature matching is crucial when tackling downstream geometric tasks such as accurate camera registration far from database images or street-to-aerial urban structure recovery [13] in standard SfM pipeline, where existing methods struggle to perform well [37].

To tackle geometry deformation induced by scale and viewpoint variation across images, tremendous efforts have been made within local feature matching pipelines. Methods directly performing convolution upon multi-scale images such as KeyNet [3] and HDDNet [5], or implicitly applying multi-scale detection such as ASLfeat [23] and DenseNet [21] are intended to mimic conventional scale space theory. Other approaches tend to mitigate scale and viewpoint change by predicting a co-visible area [35], estimating the scale distribution [4], or simply regressing warping deformation [6, 24]. Although these approaches have improved feature matching performance by considering scale and viewpoint change, they can't acquire smooth relative geometry deformation including both scale and viewpoint within a single pipeline.

Inspired by the above consideration, we present AdaMatcher, a geometry aware local feature matching approach targeting at mitigating potential geometry mismatch between image pairs without multi-scale aggregation, scale-alignment preprocessing or viewpoint warpping. Different from dual-softmax or optimal transport in LoFTR [33] which guarantees one-to-one correspondence,

we allow many-to-one assignment at patch-level matching. Putative many-to-one matches can capture sufficient image features when scale or viewpoint variation is significant to prevent patch information losses by exclusive one-to-one matching. The smooth scale transition from many-to-one matches between image pairs can be adopted to resolve scale inconsistencies. Furthermore, the structure of our delicately designed feature interaction module allows for simultaneously estimating the co-visible area probability map, which can filter out matches outside co-visible areas.

To summarize, we aim to provide several critical insights of matching local features across scales and viewpoints:

- We propose a detector-free matching approach AdaMatcher by offering a *plug-and-play* assignment strategy that allows a patch-level adaptive assignment followed by a sub-pixel refinement to guarantee the establishment of geometry aware feature correspondences.
- We introduce a query embedding to decode shared region across image pair, and help to predict probability map of this co-visible area.
- Extensive experiments and analysis demonstrate that AdaMatcher outperforms various strong baselines and achieves SOTA results for many downstream vision tasks.

## 2 Related Work

### 2.1 Scale-invariant local feature

Generally, putative feature matches are established from exhaustive or approximate [1] search in descriptor space. Mutual ratio test [22] is then applied to guarantee one-to-one discriminative matches. Finally, statistical filtering methods such as RANSAC [11] are adopted to enforce geometric constraints. Milestone hand-crafted local features such as SIFT [22] and ORB [28] explicitly model scale invariance conforming to scale space theory [37], which tackle feature matching at similar scales fundamentally. This hypothesis is inconsistent with smooth scale transition in real-world scenarios, leading to cross-scale feature mismatches. Recently, Convolutional Neural Networks (CNNs) which possess inductive bias of translation equivariance and locality has been found well suited for local feature extraction. For ASLFeat [23], local shape transformations are modeled by DCN and multi-scale feature hierarchy. However, descriptors extracted locally from low-level image textures possess poor discrimination ability. So recent data-driven approaches tend to match multi-scale CNN or Transformer-based features and rely on flexible receptive fields to acquire reliable descriptors.

### 2.2 Viewpoint-invariant local feature

Traditionally, descriptors’ scale-invariant ability gains more attention in local feature extraction; however, in many downstream tasks such as geo-localization, robustness to viewpoint change is also challenging. GeoWarp [6] directly warps

pairwise images to a closer geometrical space to eliminate viewpoint inconsistencies and then computes their similarities using deep, dense local features for image retrieval tasks. OETR [35] estimates overlap area as a preprocessing module in image matching pipeline to constrain feature extraction in the co-visible area, and eliminate scale and viewpoint inconsistencies. These studies provide important insights for our design on viewpoint-invariant feature matching.

### 2.3 Dense local feature

Due to the increasing prevalence of joint learning of keypoints and descriptors, recent data-driven approaches have shifted from local patches to image-level densely extracted features, so scale estimation from patches is not required anymore. NCNet [27] and its follow-ups [16, 26] propose a 4D matching cost volume to enumerate all possible correspondences and obtain dense matches end-to-end. Although all the potential matches are considered in the 4D matching tensor, the receptive field of 4D convolution is still limited to each match’s neighborhood area. Benefiting from the global receptive field and long-range dependencies from Transformers, LoFTR [33] extends neighborhood consensus to the whole image, setting the SOTA performance for dense feature matching approaches.

## 3 Methods

In this section, we describe our local feature matching method that benefits from an adaptive assignment strategy, named AdaMatcher as shown in Fig. 2.

### 3.1 Feature Interaction and Co-visible Area Segmentation (FICAS)

Given image pair  $I^A$  and  $I^B$ , a simple convolutional architecture (ResNet-FPN) can be used to extract patch-level and pixel-level feature maps, denoted as  $(F_{1/2}^A, F_{1/2}^B)$  and  $(F_{1/8}^A, F_{1/8}^B)$ , whose down-sampling ratios are 2 and 8 respectively.  $F_{1/8}^A$  and  $F_{1/8}^B$  are then fed into FICAS module to interact with each other and perform co-visible area segmentation.

**Preliminaries: Attentional Graph Neural Network.** SuperGlue [30] is the first to propose Attentional Graph Neural Network in image matching task, implemented by stacking nine sets of self and cross attention layers. The self-attention layer is used to exchange feature information within one image, and the cross-attention layer is used to communicate information across image pair. Although attentional feature interaction module is effective in matching tasks, is still suffers from excessive computational cost, due to the quadratic complexity of transformer. So, many efforts have been made to improve its efficiency. LoFTR [33] uses linear attention instead of the original attention layer. SGMNet [8] constructs a set of seed matches to simplify the attentional graph.



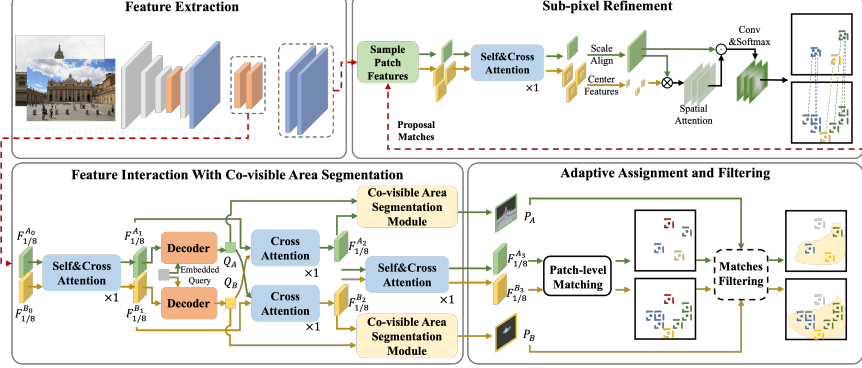


Fig. 2: **Architecture of AdaMatcher.** A local feature CNN (ResNet-FPN) extracts two feature maps with size 1/2 and 1/8 of the input image dimension. Afterwards, 1/8 coarse features from two images are interacted by self/cross attention and query embedding, followed by an overlap area segmentation module to extract co-visible area shared between two images. Then the interacted feature patches and co-visible probability maps are fed into a many-to-one assignment and filtering module, yielding sufficient patch-level matches. Finally, match proposals are sampled in the 1/2 pixel-level feature maps with a scale alignment to mitigate scale mismatch, followed by sub-pixel refinement.

**Feature Interaction with Co-visible Feature Decoding.** When humans match two images, we first look back-and-forth to find the co-visible areas, then zoom into to match local details. Therefore, we introduce a learnable query embedding between self/cross attention layers to represent information from co-visible areas, which is inspired by DETR [7]. The decoded query features are then interacted with features from the other image.

In detail, we first use one self/cross attention layer as the feature encoder to acquire information within and across images. The output features are denoted as  $F_{1/8}^{A_1}$  and  $F_{1/8}^{B_1}$  respectively. Then we adopt one query  $Q \in \mathbb{R}^{1 \times d}$  to embed co-visible context, where  $d$  is the channel dimension of query, and perform one cross-attention layer to decode the locations of the co-visible region. We take the inspiration from DETR to design this architecture, however to reduce computation cost linear attention is introduced here to replace vanilla Transformer attention. We use  $Q^A$  and  $Q^B$  to denote the features decoded from  $F_{1/8}^{A_1}$  and  $F_{1/8}^{B_1}$  respectively, i.e.,

$$Q^i = \text{Transfomer}(q = Q, k = v = F_{1/8}^{i_1}), i \in \{A, B\}. \quad (1)$$

Following that, we perform one cross-attention layer to correlate features between  $F_{1/8}^{A_1}$  and  $Q^B$ , also between  $F_{1/8}^{B_1}$  and  $Q^A$ . Output features after the interaction are denoted as  $F_{1/8}^{A_2}$  and  $F_{1/8}^{B_2}$  respectively. Assuming the network has already focused on co-visible region of the two feature maps, the next step

is to find potential matches for each features. As mentioned in SuperGlue, using global contextual cues rather than information limited to nearby locations can help to matches more accurately. Thus, we use another self/cross attention layer to construct a complete graph for feature correlation between  $F_{1/8}^{A_2}$  and  $F_{1/8}^{B_2}$ , and the output feature maps are denoted as  $F_{1/8}^{A_3}$  and  $F_{1/8}^{B_3}$ , respectively.

**Co-visible area segmentation.** Co-visible area segmentation is intend to predict commonly seen area between two images, to filter potential outliers outside co-visible area. Here we consider co-visible area segmentation as predicting a logit probability map, whose values at each pixel represent the probability of being in the co-visible region, as show in Fig.3.

We project the decoded features  $Q^{A,B}$  to construct a weight map using cross multiplication and a sigmoid function. The weight map is used to enhance the co-visible context in feature maps  $F_{1/8}^{A_2}, F_{1/8}^{B_2}$ . Then a convolution operation with the kernel size of  $3 \times 3$  and a sigmoid function are introduced, which is detailed in Eq. (2):

$$\begin{aligned} \text{weight}_i &= \text{Sigmoid}((F_{1/8}^{i_2})^T Q^i), \\ P_i &= \text{Sigmoid}(\text{Conv}(\text{weight}_i \odot F_{1/8}^{i_2} + F_{1/8}^{i_2})), \end{aligned} \quad (2)$$

where  $i \in \{A, B\}$ ,  $\odot$  denotes element-wise multiplication and  $P_A, P_B$  denote the co-visible probability map of image  $A$  and image  $B$ . After obtaining  $P_A$  and  $P_B$ , a confidence threshold can be applied to retain the co-visible area in image  $A$  and image  $B$ .



Fig. 3: Co-visible area segmentation visualizations.

### 3.2 Adaptive Assignment for Patch-level Matching

In this section, we will elaborate one of the main contributions in our work: adaptive assignment when matching between features across images. On one hand, when allowing many-to-one assignment at the patch level feature matching, we are capable of alleviating feature mismatch when large scale or view-point change

exists. On the other hand, for supervised feature matching learning, ground-truth matches obtained from camera poses and depth maps should obey mutual nearest neighbors constraint (which also named one-to-one assignment). However, when scale varies or viewpoint changes, centers of several patches within one image may be projected into only one patch of the other image, named many-to-one correspondences, as shown in Fig. 4(a). For the ground truth labels obtained by one-to-one assignment, only the correspondences that satisfy the mutual nearest neighbors constraint are taken as positive samples, while the others as negative samples. Such ambiguous label assignment is detrimental to supervised training. As shown in Fig.4(b), while a set of patch centers (or pixels) of image  $A$ :  $\{P_i^A | p_{ik}^A, k = 1, 2, \dots, N\}$  are all projected into a patch (or pixel) of image  $B$ :  $p_j^B$  using ground-truth camera poses and depth maps, features corresponding to  $\{P_i^A\}$  are similar to the feature corresponding to  $p_j^B$ . Following mutual nearest neighbors constraint,  $(p_{im}^A, p_j^B)$  would be assigned as positive sample, while  $\{(p_{ik}^A, p_j^B) | k = 1, 2, \dots, N, k \neq m\}$  are assigned as negative, where  $m = \arg \min_k \|D(W(p_{ik}^A), p_j^B)\|$ ,  $D(\cdot)$  is the projected distance between matching candidates and  $W(\cdot)$  demonstrates the projection function. Such one-to-one assignment criterion will make good correspondences into negative samples. Instead, many-to-one assignment will make correspondences  $\{(p_{ik}^A, p_j^B) | k = 1, 2, \dots, n\}$  being positive samples since their appearances are similar and they also conform to geometric constrain.

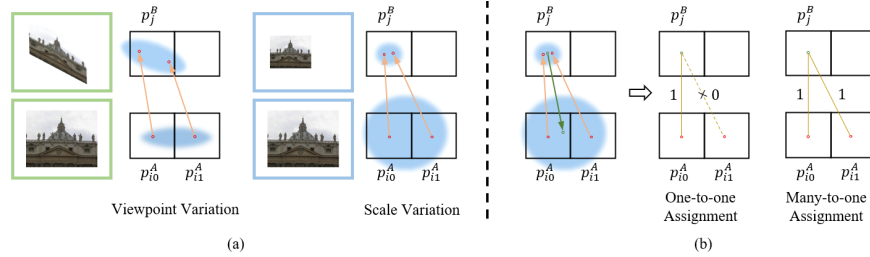


Fig. 4: **Comparison of one-to-one and many-to-one assignment.** (a) shows patch-level many-to-one matching due to viewpoint and scale changes; (b) shows the difference between many-to-one and one-to-one assignment: one-to-one only keep a single match while both  $p_{i0}^A$  and  $p_{i1}^A$  correspond to  $p_j^B$ , and many-to-one assignment keep common area matches to disambiguate positive and negative samples, to resolve geometry deformation.

**Assignment matrix formulation.** Given FICAS features  $F_{1/8}^{A_3}$  and  $F_{1/8}^{B_3}$ , we calculate their similarity matrix  $\mathcal{S}$  by  $\mathcal{S}(i, j) = \frac{1}{r} \cdot \langle F_{1/8}^{A_3}(i), F_{1/8}^{B_3}(j) \rangle$ , where  $i$  and  $j$  are index of feature patches in  $I^A$  and  $I^B$  respectively, and  $\langle \cdot, \cdot \rangle$  denotes inner product. Many-to-one assignment is a one-way operation, i.e., we assign "many"

patches on images with a large co-visible area to "one" patch on images with a small co-visible area. Hence, we apply softmax operation to similarity matrix  $\mathcal{S}(i, j)$  on two dimensions separately, followed by selecting similar matches with a threshold  $\theta_m$ :

$$\begin{aligned}\mathcal{P}_0 &= \mathbf{softmax}(\mathcal{S}(i, \cdot))_j, \quad \mathcal{M}_0 = \{(\tilde{i}, \tilde{j}) | \mathcal{P}_0(\tilde{i}, \tilde{j}) > \theta_m\}, \\ \mathcal{P}_1 &= \mathbf{softmax}(\mathcal{S}(\cdot, j))_i, \quad \mathcal{M}_1 = \{(\tilde{i}, \tilde{j}) | \mathcal{P}_1(\tilde{i}, \tilde{j}) > \theta_m\},\end{aligned}\tag{3}$$

where  $\mathcal{P}_0$  is the matching probability matrix obtained by softmax operation along the first dimension,  $\mathcal{P}_1$  is the matching probability matrix obtained by softmax operation along the zeroth dimension,  $\mathcal{M}_0$  and  $\mathcal{M}_1$  are the corresponding patch-level match proposals. Then we select the matching probability matrix  $\mathcal{P}$  and the proposal matches  $\mathcal{M}$  by:

$$\begin{aligned}\mathcal{M} &= \mathbf{Filtering}(\mathcal{M}_{index}, P_A, P_B, \theta_{co-visible}), \\ \mathcal{P} &= \mathcal{P}_{index},\end{aligned}\tag{4}$$

where  $index$  is the largest scale between image pairs, as  $index = \arg \max_k \{s_k | k = 0, 1\}$ , and  $s_0 = \frac{\mathbf{len}(\mathcal{M}_0)}{\mathbf{len}(\mathbf{unique}(\mathcal{M}_0[:, 1]))}$ ,  $s_1 = \frac{\mathbf{len}(\mathcal{M}_1)}{\mathbf{len}(\mathbf{unique}(\mathcal{M}_1[:, 0]))}$  are the scale of  $I^A$  and  $I^B$ . And **Filtering** is to filter out matches outside predicted co-visible areas, and  $\theta_{co-visible}$  is used to select pixels in the co-visible probability maps belong to the co-visible region.

### 3.3 Sub-pixel Refinement Module

By adaptive assignment we obtain match proposals through scales and views, then we refine them to final sub-pixel level matches, by a scale-alignment and an expectation regression module.

**Scale-alignment.** With match proposals from adaptive assignment, patch features are sampled in  $F_{1/2}^A$  and  $F_{1/2}^B$ . Suppose  $p_i^A$  is larger than  $p_j^B$ , match proposals are  $\{(p_{ik}^A, p_j^B) | k = 1, 2, \dots\}$ . Then one self/cross attention layer transforms patches within sampled features. The scale ratio  $s = \max(s_0/s_1, s_1/s_0)$  could be calculated from eq3.2, smaller scale images feature are upsampled by this scale ratio to compensate for scale mismatch between images.

**Sub-Pixel level regression.** To measure accurate sub-pixel level position, we correlate the center features of  $F_{ik}^A, k = 1, 2, \dots$  with upsampled feature  $F_j'^A$  to produce a heatmap representing the matching probability of each pixel in  $i$  with  $j$ . Firstly, we use the center features of  $F_{ik}^A, k = 1, 2, \dots, n$  and the upsampled features  $F_j'^A$  to calculate  $n$  spatial attention maps. Then we perform a dot-product operation on the attention maps and  $F_j'^A$  to implement the spatial attention mechanism. Finally, a simple convolution and softmax operation is employed to generate location distribution. The expectation over the probability

distribution is the final position  $i'$  with sub-pixel accuracy on  $I_A$ . By this scale-aware adaption to match position refinement, we achieve more accurate sub-pixel matches.

### 3.4 Supervision

**Co-visible Area Segmentation Loss.** For the co-visible area segmentation, we treat it as a per-pixel binary classification task. The loss  $\mathcal{L}_{co-visible}$  can be calculated by focal loss [19] (abbr. as  $FL$  hereafter):

$$\mathcal{L}_{co-visible} = FL(P_A, \hat{P}_A) + FL(P_B, \hat{P}_B), \quad (5)$$

where  $\hat{P}_A$  and  $\hat{P}_B$  denote the ground-truth co-visible areas of image  $A$  and image  $B$ , respectively.

**Proposal Matching Loss.** For the loss function of the adaptive many-to-one matching probability matrix  $\mathcal{P}$ , we also use focal loss [19]:

$$\mathcal{L}_{M2O} = FL(\mathcal{P}, \tilde{\mathcal{P}}). \quad (6)$$

where  $\tilde{\mathcal{P}}$  is the ground-truth labels of the many-to-one matching probability matrix calculated from the camera poses and depth maps, and  $\mathcal{P}$  is the predicted matching probability matrix.

**Refinement Loss.** Inspired by LoFTR [33], we use the same loss function for the final predicted matches. However, considering possible inaccurate camera poses or incomplete depth maps in the dataset, we introduce a epipolar loss as in [34] for the predicted matches with epipolar distances less than  $w^*$ , resulting in final refinement loss as:

$$\mathcal{L}_{refine} = \begin{cases} \frac{1}{|\mathcal{M}_{gt}^0|} \sum_{i,j'} \frac{1}{\sigma(i)^2} \|j' - j'_{gt}\| + \frac{1}{|\mathcal{M}_{ep}^0|} \sum_{i,j'} \frac{1}{\sigma(i)^2} \left\| \frac{\mathcal{L}_{ep}(i,j')}{w^*} \right\|, & \text{if } index=0 \\ \frac{1}{|\mathcal{M}_{gt}^1|} \sum_{i',j} \frac{1}{\sigma(j)^2} \|i' - i'_{gt}\| + \frac{1}{|\mathcal{M}_{ep}^1|} \sum_{i',j} \frac{1}{\sigma(j)^2} \left\| \frac{\mathcal{L}_{ep}(j,i')}{w^*} \right\|, & \text{otherwise} \end{cases}, \quad (7)$$

where  $M_{gt}^0$  and  $M_{gt}^1$  are the ground-truth matches calculated from ground-truth depths and camera poses,  $M_{ep}^0$  and  $M_{ep}^1$  are the predicted matches with epipolar distances less than  $w^*$ ,  $\mathcal{L}_{ep}$  is the epipolar loss, and the  $index$  is calculated in Eq.(3.2). Our final loss is balanced as:

$$\mathcal{L} = 0.5 * \mathcal{L}_{co-visible} + 1.0 * \mathcal{L}_{M2O} + 1.0 * \mathcal{L}_{Refine}. \quad (8)$$

### 3.5 Implementations

We train AdaMatcher on the MegaDepth datasets following [33], without any data augmentation. The network is trained using AdamW optimizer with initial

learning rate of  $8 \times 10^{-3}$  and batch size of 32. It converges after 15 hours of training on 32 V100 GPUs. The image feature extractor is a standard ResNet-FPN [12, 18] architecture, which is identical to LoFTR [33]. We use the Linear attention mechanism [15] to implement the self/cross transformer layer.  $\theta_m$  is set to 0.5,  $\theta_{co-visible}$  is set to 0.2 and the base window size  $w = 5$ . The number of channels of the  $F_{1/8}$  and  $F_{1/2}$  is 256 and 128, respectively. To save GPU memory usage during training, we sample 30 percent of matches (max to 2500) from the match proposals for supervision in one-to-one sub-pixel refinement module.

## 4 Experiments

In the following sections, we evaluate our methods across several practical scenarios, including image matching and visual localization.

### 4.1 Homography Estimation

**Dataset:** HPatches [2] is the most widely used image matching evaluation dataset. There are 116 scenes and each scene has 6 images, where first image is paired with remaining five images. Following [10], we split out 52 sequences with large illumination variations and 56 sequences under significant viewpoint changes, to evaluate our method under different circumstances.

**Metrics:** Following [9, 30, 38] we use corner correctness to describe the performance of estimated homography. Four corners in the first reference image are wrapped to the other image by estimated homography. Then percentage of correct estimated homographies whose average error of the four corners is less than  $1/3/5$  pixels demonstrates the matching *Accuracy*. We use OpenCV RANSAC as the robust estimator to compute the homography estimation following [38]. Considering that HPatches exhibit only homography transformation which can not comprehensively reflect the performance in real applications, we resort to more advanced downstream geometrical tasks in the following sections.

**Results:** We split matching methods into "Detector-based" and "Detector-free" as in LoFTR [33]. Tab.1 shows that AdaMatcher notably performs on par with or better than other baselines under all error thresholds. For illumination changes, detector-free methods often outperform detector-based methods, except for Patch2Pix [38] which adopts Detector-free method NCNet [27] to predict patch-level match proposals. Under viewpoint variations, detector-based methods perform better, maybe due to more accurate extracted keypoint positions. But after added M2O with superpoint and superglue, AdaMatcher still performs better than other detector-based methods. Overall, AdaMatcher performs consistently better than strong baseline LoFTR under almost all circumstances. Compared with LoFTR [33] which used one-to-one assumptions, AdaMatcher used many-to-one coarse matches which eliminate matching ambiguity from supervision and inference.

Table 1: **Homography estimation on HPatches**. Images are resized to their longer dimensions equal to 840 and we limit the maximum amount of matches for the above methods to 1K. The better methods are underlined, and the best overall method is highlighted in bold

Category	Method	Overall			Illumination			Viewpoint		
		Accuracy(% , $\epsilon < 1/3/5\text{px}$ )								
Detector-based	SP [9]+NN	0.31	/0.66	/0.78	0.45	/0.81	/0.92	0.18	/0.51	/0.64
	R2D2 [25]+NN	0.29	/0.60	/0.72	0.40	/0.77	/0.87	0.18	/0.43	/0.58
	SP [9]+CAPS [34]+NN	0.27	/0.66	/0.71	0.39	/0.79	/0.89	0.15	/0.53	/0.65
	Patch2Pix [38]	0.34	/0.68	/0.79	0.53	/0.89	<u>0.96</u>	0.16	/0.47	/0.63
	SP [9]+SG [30]	0.34	/0.67	/0.81	0.47	/0.81	/0.91	0.21	/0.53	<b>0.72</b>
	SP [9]+SG [30]+M2O	0.35	/0.71	/0.81	0.46	/0.83	/0.91	<u>0.24</u>	<b>0.59</b>	<b>0.72</b>
Detector-free	LoFTR-OT [33]	0.41	/0.68	/0.78	0.68	/0.94	<b>0.98</b>	0.15	/0.43	/0.59
	LoFTR-DS	<u>0.44</u>	<u>/0.73</u>	<u>/0.82</u>	<u>0.71</u>	<u>/0.93</u>	<b>0.98</b>	0.19	/0.54	/0.67
	AdaMatcher	<b>0.49</b>	<b>/0.75</b>	<b>/0.83</b>	<b>0.73</b>	<b>/0.94</b>	<b>0.98</b>	<b>0.26</b>	<u>0.57</u>	<u>/0.69</u>

## 4.2 Relative Pose Estimation

**Datasets:** We use MegaDepth [17] to demonstrate the effectiveness of AdaMatcher for pose estimation in outdoor scenes. Following OETR [35], we used a scale-split MegaDepth test set (with 10 scenes), as scale ratio ranges in  $[1, 2)$ ,  $[2, 3)$ ,  $[3, 4)$ ,  $[4, +\infty)$ . Fig.5 qualitatively shows the matching result of LoFTR and AdaMatcher in MegaDepth. During validation, images are resized with a longer side to 840.

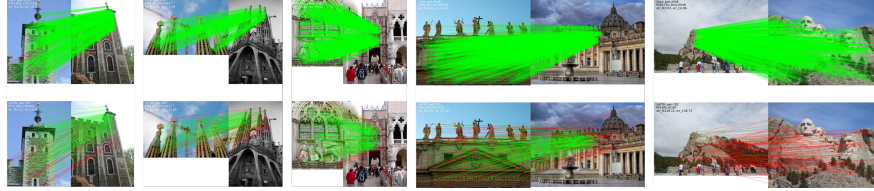


Fig. 5: **Qualitative results**. AdaMatcher (top row) is compared to LoFTR in MegaDepth datasets. AdaMatcher obtains dense matches with epipolar error beyond  $1 \times 10^{-4}$  as shown in green lines. In large scale difference, LoFTR (bottom row) with more mismatches as shown in red lines.

**Metrics:** Following [30], we report the **AUC** of the pose error under thresholds ( $5^\circ$ ,  $10^\circ$ ,  $20^\circ$ ), where the pose error is set as the maximum angular error of relative rotation and translation. In our evaluation protocol, the relative poses are recovered from the essential matrix, estimated from feature matching with RANSAC. We also report match precision in normalized camera coordinates, with epipolar distance threshold of  $1e^{-4}$  [9, 10, 30].

**Results on MegaDepth:** When the relative scale ratio is small, the performance of AdaMatcher can only catch up with LoFTR. However, as the scale difference increases, AdaMatcher outperforms its counterparts more obviously. Though R2D2 [25] utilizes multi-scale images to inference features and ASLFeat [23] extracts features from multi-scale score maps, these methods cannot model relative scale ratio between images like AdaMatcher. LoFTR fixes keypoints position in reference images, and for every coarse matching patch, it calculates the expectation of correlation heatmap to extract sub-pixel keypoints. When the scale differences between image pairs are large, the number of matches in the coarse-level will be decreased, which could harm performance.

Table 2: **Evaluation on MegaDepth.** Performance gain from AdaMatcher becomes more prominent when scaling variation between image pairs increases

Methods	Scale [1,2)			Scale [2,3)			Scale [3,4)			Scale [4,inf)		
	AUC@5°			AUC@10°			AUC@20°					
R2D2 [25]	37.84	/55.90	/70.66	22.67	/36.93	/51.88	6.63	/13.02	/22.01	2.13	/4.02	/7.18
ASLFeat [23]	33.80	/50.33	/65.12	21.87	/35.41	/49.68	8.53	/16.01	/26.50	2.95	/6.32	/11.84
SP [9]+SG [30]	50.37	/67.51	/79.81	40.54	/58.31	/72.64	19.93	/34.80	/51.61	10.61	/19.98	/34.16
LoFTR [33]	60.15	/74.68	/84.45	49.69	/65.72	/77.94	24.86	/39.67	/55.08	10.16	/18.74	/29.97
AdaMatcher	<b>60.47</b>	<b>/75.19</b>	<b>/85.06</b>	<b>52.01</b>	<b>/67.60</b>	<b>/79.17</b>	<b>33.21</b>	<b>/49.54</b>	<b>/64.73</b>	<b>19.12</b>	<b>/32.08</b>	<b>/46.61</b>

**Refinement Module:** As mentioned before, many-to-one could be treated as a refinement module with different extractors and matchers as patch2Pix [38]. Different from SuperGlue mutual nearest neighbors constraint, we calculate row matches and column matches separately to get a many-to-one and one-to-many matches, and then, refine sub-pixel level position in descriptor feature map.

Table 3: **Comparison of adding M2O with SOTA matchers(SP+SG).** After adding M2O as a refinement module with SP+SG in different megadepth scale datasets, AUC metric has some improvement

Methods	Scale [1,2)			Scale [2,3)			Scale [3,4)			Scale [4,inf)		
	AUC@5°			AUC@10°			AUC@20°					
SP [9]+SG [30]	50.43	/67.64	/79.97	39.41	/57.78	/72.34	19.72	/35.22	/51.97	10.09	/19.62	/33.88
SP [9]+SG [30]+M2O	<b>53.56</b>	<b>/70.01</b>	<b>/81.90</b>	<b>42.32</b>	<b>/59.51</b>	<b>/73.77</b>	<b>23.77</b>	<b>/39.55</b>	<b>/56.08</b>	<b>12.63</b>	<b>/23.68</b>	<b>/37.59</b>

### 4.3 Visual Localization

**Datasets:** In HPatches and MegaDepth we only recover relative pose from feature matches. For real-world applications such as AR navigation or autonomous driving, visual localization with absolute pose estimation is a more important



geometrical task. Aachen Day-Night v1.1 dataset [36] is chosen to demonstrate the visual localization ability of AdaMatcher. The benchmark [31, 32] has 6697 reference images and 1015 query images (824 daytime, 191 nighttime), with the evaluation of local feature matching for day-night localization tasks under larger viewpoints and illumination changes.

**Experimental setup:** We use open-sourced hierarchical localization pipeline HLoc proposed in [29] to evaluate on day-night query images. AdaMatcher should first plugged into the pipeline and build a 3D model from estimated 2D matches. Different from detector-based methods which extract keypoints before matching and naturally depend on the image itself, detector-free methods extract features conditioned on two images. As such, feature positions extracted in image A conditioned on image A+B might differ slightly to those extracted in image A conditioned on image A+C. So in order to complete feature triangulation, we quantize matches by representative keypoints that are closer than 4 pixels to each other with their mean location as in [38]. To prevent quantization drift, the max offset is limited to 24 pixels. After quantization, we remove duplicated matches and keep only the one with the highest confidence score. Obviously, it is not a perfect solution with degraded pixel-level accuracy, but should be a reasonable metric to the evaluation of our AdaMatcher.

Table 4: **Visual localization evaluation on the Aachen Day-Night [36] benchmark v1.1**

Method	Day			Night		
	(0.25m, 2°) / (0.5m, 5°) / (1.0m, 10°)			(0.25m, 2°) / (0.5m, 5°) / (1.0m, 10°)		
SuperPoint [9]+SuperGlue [30]	<b>89.8</b>	<b>96.1</b>	<b>99.4</b>	77.0	90.6	<b>100.0</b>
SuperGlue+Patch2Pix [38]	89.3	95.8	99.2	78.0	90.6	99.0
Patch2Pix	86.4	93.0	97.5	72.3	88.5	97.9
LoFTR-DS [33]	-	-	-	72.8	88.5	99.0
LoFTR-OT [33]	88.7	95.6	99.0	78.5	90.6	99.0
AdaMatcher	<u>89.2</u>	<u>96.0</u>	<u>99.3</u>	<b>79.1</b>	<b>90.6</b>	<u>99.5</u>

**Results:** As shown in Tab. 4, for local feature evaluation on night-time circumstances, AdaMatcher outperforms all other methods (slightly lower than SuperPoint [9] + SuperGlue [30] within error tolerance of 1.0m and 10°). This can be probably ascribed to the superior robustness of efficient Transformer-based architecture. On the other hand, AdaMatcher outperforms other methods on day-time queries besides SuperGlue.

#### 4.4 Ablation Study

To fully understand different modules in AdaMatcher and evaluate different design choices, we repeat outdoor experiments on MegaDepth with scale ranges in  $[2, +\infty)$ , as shown in Tab.5. The first row is the result of our baseline method

Table 5: **Ablation of AdaMatcher.** AdaMatcher recovers a more accurate relative pose compared to baseline method LoFTR and all parts are useful modules that bring noticeable performance gain for AdaMatcher

Sub Modules				Pose Estimation AUC				Precision	
EL	FICAS	M2O	Refine	@5°	$\Delta$	@10°	$\Delta$	@20°	$\Delta$
				28.20	-	41.34	-	54.30	-
✓				28.46	+0.26	41.77	+0.43	54.86	+0.56
✓	✓			29.65	+1.45	43.42	+2.08	56.66	+2.36
✓	✓			30.60	+2.40	44.51	+3.17	57.40	+3.10
✓	✓	✓	✓	32.62	+4.42	47.24	+5.90	60.87	+6.57
✓	✓	✓	✓	35.22	+7.02	50.08	+8.74	63.68	+9.38
				72.28	-	71.38	-0.90	74.22	+1.94
				73.16	+0.88	81.37	+9.09	83.53	+11.25

LoFTR [33], 'EL' indicates that epipolar loss is added to LoFTR, 'FICAS' represents the LoFTR module (four sets of self- and cross- attention layers) is replaced with our FICAS (Section 3.1), 'M2O' denotes replacing LoFTR's coarse-level matching with our many-to-one assignment (Section 3.2), and 'Refine' denotes replacing LoFTR's fine-level matching with our one-to-one refinement module (Section 3.3). From the results of the above experiments, epipolar loss can slightly improve the accuracy of relative pose estimation. By using FICAS module, we can get more accurate matches. While allowing many-to-one assignment in patch-level matching, the accuracy of relative pose estimation and the precision of matching are greatly improved, which means that many-to-one assignment plays a vital role here. And the performance can be further enhanced by adding our one-to-one refinement module to AdaMatcher.

## 5 Conclusions

In this paper, we find the conventional mutual nearest neighbour standard should bottleneck the final performance during patch-level or pixel-level matching. The proposed AdaMatcher allows for many-to-one assignment during patch-level matching, which overcomes the ambiguous underlying ground-truth label assignments, and enable estimation of the scale ratio between given image pair. We observe a noticeable performance boost, especially when the scale or view-point between image pairs varies. Also we introduce query embedding in feature interaction to decode the positions of co-visible area and then filter out possible false matches. Particularly, by plugging a dedicated one-to-one refinement module, we can effectively achieve scale alignment and accurate sub-pixel position regression. We have conducted extensive experiments to study the effect of our findings and demonstrated the superiority of our proposed AdaMatcher. We believe that AdaMatcher will bring new insights to the feature matching community.

## References

1. Aiger, D., Kokiopoulou, E., Rivlin, E.: Random grids: Fast approximate nearest neighbors and range searching for image search. ICCV (2013)
2. Baltas, V., Lenc, K., Vedaldi, A., Mikolajczyk, K.: HPatches: A benchmark and evaluation of handcrafted and learned local descriptors. CVPR (2017)
3. Barroso-Laguna, A., Riba, E., Ponsa, D., Mikolajczyk, K.: Key. net: Keypoint detection by handcrafted and learned cnn filters. ICCV (2019)
4. Barroso-Laguna, A., Tian, Y., Mikolajczyk, K.: ScaleNet: A Shallow Architecture for Scale Estimation. Arxiv: (2021)
5. Barroso-Laguna, A., Verdie, Y., Busam, B., Mikolajczyk, K.: Hdd-net: Hybrid detector descriptor with mutual interactive learning. ACCV (2020)
6. Berton, G., Masone, C., Paolicelli, V., Caputo, B.: Viewpoint invariant dense matching for visual geolocalization. ICCV (2021)
7. Carion, N., Massa, F., Synnaeve, G., Usunier, N., Kirillov, A., Zagoruyko, S.: End-to-end object detection with transformers”. ECCV (2020)
8. Chen, H., Luo, Z., Zhang, J., Zhou, L., Bai, X., Hu, Z., Tai, C.L., Quan, L.: Learning to match features with seeded graph matching network. ICCV (2021)
9. DeTone, D., Malisiewicz, T., Rabinovich, A.: Superpoint: Self-supervised interest point detection and description. CVPR (2018)
10. Dusmanu, M., Rocco, I., Pajdla, T., Pollefeys, M., Sivic, J., Torii, A., Sattler, T.: D2-net: A trainable cnn for joint description and detection of local features. CVPR (2019)
11. Fischler, M.A., Bolles, R.C.: Random sample consensus: a paradigm for model fitting with applications to image analysis and automated cartography. Communications of the ACM (1981)
12. He, K., Zhang, X., Ren, S., Sun, J.: Deep residual learning for image recognition. CVPR (2016)
13. Hu, S., Feng, M., Nguyen, R.M.H., Lee, G.H.: CVM-Net : Cross-View Matching Network for Image-Based Ground-to-Aerial. CVPR (2018)
14. Jiang, W., Trulls, E., Hosang, J., Tagliasacchi, A., Yi, K.M.: COTR: Correspondence Transformer for Matching Across Images. ICCV (2021)
15. Katharopoulos, A., Vyas, A., Pappas, N., Fleuret, F.: Transformers are RNNs: Fast Autoregressive Transformers with Linear Attention. ICML (2020)
16. Li, X., Han, K., Li, S., Prisacariu, V.: Dual-resolution correspondence networks. NeurIPS (2020)
17. Li, Z., Snavely, N.: MegaDepth: Learning Single-View Depth Prediction from Internet Photos. CVPR (2018)
18. Lin, T.Y., Dollár, P., Girshick, R., He, K., Hariharan, B., Belongie, S.: Feature pyramid networks for object detection. CVPR (2017)
19. Lin, T.Y., Goyal, P., Girshick, R., He, K., Dollar, P.: Focal loss for dense object detection. ICCV (2017)
20. Lindeberg, T.: Feature Detection with Automatic Scale Selection. IJCV (1998)
21. Liu, D., Cui, Y., Yan, L., Mousas, C., Yang, B., Chen, Y.: Densernet: Weakly supervised visual localization using multi-scale feature aggregation. AAAI (2021)
22. Lowe, D.G.: Distinctive image features from scale-invariant keypoints. IJCV (2004)
23. Luo, Z., Zhou, L., Bai, X., Chen, H., Zhang, J., Yao, Y., Li, S., Fang, T., Quan, L.: ASLFeat: Learning local features of accurate shape and localization. CVPR (2020)
24. Parihar, U.S., Gujarathi, A., Mehta, K., Tourani, S., Garg, S., Milford, M., Krishna, K.M.: Rord: Rotation-robust descriptors and orthographic views for local feature matching. IROS (2021)

25. Revaud, J., Weinzaepfel, P., De Souza, C., Pion, N., Csurka, G., Cabon, Y., Humenberger, M.: R2d2: repeatable and reliable detector and descriptor. *NeurIPS* (2019)
26. Rocco, I., Arandjelović, R., Sivic, J.: Efficient Neighbourhood Consensus Networks via Submanifold Sparse Convolutions. *ECCV* (2020)
27. Rocco, I., Cimpoi, M., Arandjelović, R., Torii, A., Pajdla, T., Sivic, J.: Neighbourhood consensus networks. *NeurIPS* (2018)
28. Rublee, E., Rabaud, V., Konolige, K., Bradski, G.: Orb: An efficient alternative to sift or surf. *ICCV* (2011)
29. Sarlin, P.E., Cadena, C., Siegwart, R., Dymczyk, M.: From coarse to fine: Robust hierarchical localization at large scale. *CVPR* (2019)
30. Sarlin, P.E., DeTone, D., Malisiewicz, T., Rabinovich, A.: Superglue: Learning feature matching with graph neural networks. *CVPR* (2020)
31. Sattler, T., Maddern, W., Toft, C., Torii, A., Hammarstrand, L., Stenborg, E., Safari, D., Okutomi, M., Pollefeys, M., Sivic, J., et al.: Benchmarking 6dof outdoor visual localization in changing conditions. *CVPR* (2018)
32. Sattler, T., Weyand, T., Leibe, B., Kobbelt, L.: Image retrieval for image-based localization revisited. *BMVC* (2012)
33. Sun, J., Shen, Z., Wang, Y., Bao, H., Zhou, X.: Loftr: Detector-free local feature matching with transformers. *CVPR* (2021)
34. Wang, Q., Zhou, X., Hariharan, B., Snavely, N.: Learning Feature Descriptors using Camera Pose Supervision. *ECCV* (2020)
35. YingChen, D.H., ShangXu, J.L., YongLiu: Guide local feature matching by overlap estimation. *AAAI* (2022)
36. Zhang, Z., Sattler, T., Scaramuzza, D.: Reference Pose Generation for Long-term Visual Localization via Learned Features and View Synthesis. *IJCV* (2020)
37. Zhou, L., Zhu, S., Shen, T., Wang, J., Fang, T., Quan, L.: Progressive Large Scale-Invariant Image Matching in Scale Space. *ICCV* (2017)
38. Zhou, Q., Sattler, T., Leal-Taixe, L.: Patch2pix: Epipolar-guided pixel-level correspondences. *CVPR* (2021)